



THE UNIVERSITY *of* EDINBURGH

Edinburgh Research Explorer

## Influence of transition group elements on the stability of the delta- and eta-phase in nickelbase alloys

### Citation for published version:

Baeker, M, Roesler, J, Hentrich, T & Ackland, G 2017, 'Influence of transition group elements on the stability of the delta- and eta-phase in nickelbase alloys', *Modelling and simulation in materials science and engineering*, vol. 26, no. 1, 015005. <https://doi.org/10.1088/1361-651X/aa9759>

### Digital Object Identifier (DOI):

[10.1088/1361-651X/aa9759](https://doi.org/10.1088/1361-651X/aa9759)

### Link:

[Link to publication record in Edinburgh Research Explorer](#)

### Document Version:

Peer reviewed version

### Published In:

Modelling and simulation in materials science and engineering

### General rights

Copyright for the publications made accessible via the Edinburgh Research Explorer is retained by the author(s) and / or other copyright owners and it is a condition of accessing these publications that users recognise and abide by the legal requirements associated with these rights.

### Take down policy

The University of Edinburgh has made every reasonable effort to ensure that Edinburgh Research Explorer content complies with UK legislation. If you believe that the public display of this file breaches copyright please contact [openaccess@ed.ac.uk](mailto:openaccess@ed.ac.uk) providing details, and we will remove access to the work immediately and investigate your claim.



# Influence of transition group elements on the stability of the $\delta$ - and $\eta$ -phase in nickelbase alloys

Martin Bäker<sup>1</sup>, Joachim Rösler<sup>1</sup>, Tatiana Hentrich<sup>2</sup>, Graeme Ackland<sup>3</sup>

October 5, 2017

<sup>1</sup> Institut für Werkstoffe, Langer Kamp 8, 38106 Braunschweig, Germany

<sup>2</sup> VDM Metals International GmbH, Plettenberger Strasse 2, 58791 Werdohl, Germany

<sup>3</sup> School of Physics & Astronomy, The University of Edinburgh, Peter Guthrie Tait Road, Edinburgh EH9 3FD, Scotland

## Abstract

To improve the high-temperature capability of 718-type wrought nickel-base superalloys, the  $\gamma'$ -phase ( $\text{Ni}_3\text{Al}$ ) can be stabilized. However, this also reduces the size of the forging window because forging has to be done above the  $\gamma'$ - and below the solvus temperature of the phase that is used to enable fine-grain forging, i. e. the  $\delta$ -phase of  $\text{Ni}_3\text{Nb}$  type or the  $\eta$ -phase of  $\text{Ni}_3\text{Ti}$ -type. Understanding the influence of alloying elements on the formation of these phases is therefore important. In this paper, density functional theory calculations at 0K are performed to determine the stabilizing effect of aluminium and of the transition group elements on the stability of the  $\delta$ -phase and  $\eta$ -phase. Most of the transition group elements of 5th and 6th period stabilize the  $\delta$ -phase, whereas the stabilizing effect on the  $\eta$ -phase is weaker. According to the calculations, Mo, Tc, W, Re, and Os may be expected to stabilize the  $\delta$ -phase but not the  $\eta$ -phase, whereas Al and Zn strongly stabilize the  $\eta$ -phase. V, Zr, Ru, Rh, Pd, Ag, Cd, Hf, Ta, Ir, Pt, Au, and Hg stabilize both phases. For some elements (Cr, Mn, Fe, Co), magnetic effects in the  $\delta$  and especially in the  $\eta$ -phase are shown to be significant at the concentrations studied here.

**Keywords** nickel alloys, nickel-base superalloys, phase stability, density functional theory

## 1 Introduction

Alloys 718 and 706 belong to a special class of materials among the Ni-based superalloys. These so-called 718-type materials excel due to their outstanding manufacturability and high strength up to service temperatures of about 650 °C. Therefore, they are materials of choice for highly loaded turbine discs in aircraft engines amongst other components [1, 2]. Alloy 718 alone accounts for about two-thirds of the weight of superalloys in aircraft engines [3].

718-type superalloys are strengthened by the  $\gamma'$  and  $\gamma''$ -phases. These phases have to be stable at service temperature, but are dissolved during forging to ensure sufficient malleability of the alloy. Additional phases that are stable at higher temperatures are used to hinder grain growth during the forging process, thus ensuring a fine grained microstructure [4]. These phases are either the  $\delta$ -phase ( $\text{Ni}_3\text{Nb}$ , Strukturbericht designation  $\text{DO}_a$ ) or the  $\eta$ -phase ( $\text{Ni}_3\text{Ti}$ , Strukturbericht designation  $\text{DO}_{24}$ ). Consequently, 718-type superalloys are designed such that the solvus temperature of the strengthening phases is above service temperature but below forging temperature, while the  $\delta/\eta$ -phase is stable up to the forging temperature. In other words, the solvus temperature of the  $\delta/\eta$ -phase must exceed that of the strengthening phases.

Due to ever increasing temperatures in gas turbines, there is demand for 718-type alloys allowing for higher application temperatures. This requires improved stability of the strengthening phases, which can be readily achieved increasing the Al-content of the alloy as it is done in the alloy 718Plus [5] and VDM Alloy 780 [6]. However, if the  $\gamma'$  solvus temperature is increased, the forging temperature has to be increased as well. This, in turn, requires raising the thermal stability of the  $\delta/\eta$ -phase. In designing new wrought nickel-based superalloys with increased temperature stability, it is thus necessary to understand the influence of alloying elements on the stability of the  $\delta$ - and  $\eta$ -phase.

In this paper, DFT simulations at 0K are used to determine the solution energy of aluminium and transition group elements in the  $\delta$ -phase and  $\eta$ -phase to understand which elements can stabilize these phases. (Detailed

34 calculations for the influence of the most important alloying elements on the  
35  $\gamma'$ -phase can be found in [7].) These elements have been selected because the  
36 metallic alloying elements in nickelbase superalloys are either transition group  
37 elements or aluminium. The stabilizing effect on both phases is compared to  
38 aid the design of future alloys.

## 39 2 Theory and Methods

### 40 2.1 Calculation method

41 Density functional theory calculations at 0K were performed using VASP  
42 [8, 9, 10]. A plane wave bases set with projected augmented wave (PAW)  
43 pseudopotentials [11, 12] was used in the simulations together with Per-  
44 dew-Burke-Ernzerhof [13] exchange correlation functionals. Where available,  
45 pseudopotentials including full simulation of  $s$ - or  $p$ -electrons (i. e. the max-  
46 imum valency available) have been used. The energy cutoff (ENCUT) was  
47 chosen as 520 eV in all simulations, a value that is 1.3 times the largest cutoff  
48 value provided in the PBE files of all elements simulated as recommended  
49 in the VASP manual to ensure that absolute energies are calculated to high  
50 precision. Calculations were usually spin-polarized, with some exceptions for  
51 calculations within the  $\delta/\eta$ -phase where both polarized and non-polarized  
52 calculations were performed for some elements as explained below.

53 The spacing of the  $k$ -points in the reciprocal lattice was chosen as  $0.1 \text{ \AA}^{-1}$ ;  
54 resulting in  $k$ -point grids of  $9^3$  for the  $\gamma$ -cell,  $8 \cdot 13 \cdot 7$  for the  $\delta$ -cell and  $13 \cdot 8 \cdot 8$   
55 for the  $\eta$ -cell. (Each of the cells contained 32 atoms, see below.) For the  $\gamma$ -  
56 cell consisting of pure Ni, a smaller spacing of  $0.07 \text{ \AA}^{-1}$  did result in an  
57 energy difference of less than 0.01 meV per atom. For the  $\eta$ -cell, increasing  
58 the  $k$ -point grid to  $18 \cdot 11 \cdot 11$  changed the energy by less than 0.02 meV per  
59 atom. All calculations except for the pure element energies were performed  
60 for 32-atom supercell to avoid effects from different atom numbers.

61 The precision of the calculation was set to “accurate” to avoid wrap  
62 around errors; the real space operators were calculate to a precision of  $10^{-4}$   
63 (ROPT=1e-4). Intermediate runs to determine the optimum lattice paramete-  
64 rs were performed with an electronic precision of  $10^{-3}$  meV (EDIFF =1.E-6),  
65 the final runs with  $10^{-4}$  meV. The ionic loop during relaxation was stopped  
66 when the energy change was below  $10^{-2}$  meV (EDIFFG =1.E-5).

67 To check the influence of the size of the chosen 32-atom supercell and

68 possible self-interaction of the atoms, calculations with a fully relaxed larger  
69 256-atom  $\gamma$ -supercell were done for two elements, V and Nb. The substitution  
70 energies differed by 11.6 meV for V and 1.3 meV for Nb. Calculations with  
71 a 32-atom cell therefore do not correspond to the strict dilute limit.

72 For each of the considered atomic configurations, the lattice constant and  
73 lattice shape as well as the ionic positions were relaxed. To do so, we em-  
74 ployed the following two-step procedure as recommended in the VASP man-  
75 ual [14]: In a first step, calculations at fixed lattice volume were performed  
76 for five different volumes by simply changing the scale factor in the defini-  
77 tion of the initial grid. Each of these calculations was at constant volume  
78 performed with relaxation of the ions (ISIF = 2) for the  $\gamma$ -phase and with  
79 relaxation of the ions and the cell shape (ISIF = 4) for the  $\delta$  and  $\eta$ -phase.  
80 These calculations were performed with Gaussian smearing and a smearing  
81 parameter of 0.07 eV. (These values were taken from [7].)

82 A Birch-Murnaghan state equation [15] was used to fit the energies and  
83 determine the optimum scale factor. A final calculation using this scale  
84 factor was performed, using the fixed final ionic positions of the run with the  
85 closest scale factor. In this final calculation, a tetrahedral mesh with Blöchl  
86 correction was used.

87 This method results in lower energies compared to those calculated by  
88 simply relaxing the cell shape, size and ions in one step (ISIF = 3). For  
89 example, for a 32-atom  $\eta$ -phase supercell, the energy calculated using ISIF =  
90 3 and then performing a final calculation with fixed lattice and ions is 21 meV  
91 larger than the final energy obtained in the way described here; for a Ni<sub>31</sub>Nb-  
92 cell, the final energy is 39 meV larger using the direct relaxation.

## 93 2.2 Pure element calculations

94 The main purpose of this study is the comparison between the solution en-  
95 ergies in the three phases considered here ( $\gamma$ ,  $\delta$ ,  $\eta$ ). In this comparison, the  
96 energy to transport the element under consideration from one phase to an-  
97 other is calculated (see eqs. (4) and (5)) and pure element energies are not  
98 needed. Nevertheless, pure element energies allow to report substitution en-  
99 ergies for single phases and are therefore helpful as reference quantities. For  
100 Nb and Ti, calculating the energy of the pure element also serves as a check  
101 on phase stability (see section 3.3 and 3.4).

102 Most of the elements considered have a bcc, fcc or hcp lattice struc-  
103 ture. Exceptions are mercury with a rhombohedral lattice structure and

104 manganese with a complicated, 29-atom unit cell. For fcc and bcc elements,  
105 a conventional unit cell was used; for hcp elements, a 2-atom cell was em-  
106 ployed. The initial configurations of all unit cells were taken from the open  
107 quantum molecular database [16] with the exception of the 29-atom Mn cell  
108 which was taken from [17]. For Co, both an fcc and an hcp structure were  
109 calculated due to the small difference in their energy.

110 For all elements considered, the element lattice was relaxed as described  
111 in the previous section; allowing for ionic relaxation in the cubic elements  
112 and for ionic and cell shape relaxation for the hcp and the rhombohedral  
113 Hg lattice. All cells were initialized with a ferromagnetic state. The only  
114 exception was Cr where a 2-atom anti-ferromagnetic bcc configuration was  
115 used.

### 116 **2.3 Substitution in the $\gamma$ -phase**

117 A 32-atom ( $2^3$  conventional fcc) cell was used for the  $\gamma$ -phase; replacing one  
118 atom with the alloying atom under consideration. The  $\gamma$ -phase is ferromag-  
119 netic; alloying atoms may possess moment aligned with (ferromagnetic) or  
120 opposite to (ferrimagnetic) the nickel atoms.. To check for magnetic effects in  
121  $\text{Ni}_{31}\text{X}$ , calculations with the initial magnetic moment of the alloying element  
122 being aligned or opposite to that of the nickel atoms (setting the moment of  
123 this atom to  $\pm 1\mu_B$ , that of all Ni atoms to  $1\mu_B$ ) were performed, using a fixed  
124 lattice constant and slightly loosened convergence criteria to save CPU time.  
125 For most elements, both simulations converged to the same state. Exceptions  
126 were Mn and Fe, where the final configuration with an opposite moment had  
127 a considerably higher energy than the ferromagnetic configuration, Cr, where  
128 the final configuration with opposite moment is energetically favourable, and  
129 Co, where the computation with opposite moment did not converge.

130 To calculate the final energies of the  $\text{Ni}_{31}\text{X}$  supercells, the lattice con-  
131 stant was relaxed as described above. Based on the results for the ferro-  
132 and ferrimagnetic initialization as described in the previous paragraph, all  
133 configurations except for  $\text{Ni}_{31}\text{Cr}$  were initialized with a purely ferromagnetic  
134 state. It should be noted that the ferrimagnetic state of the Cr atom might  
135 change in a larger supercell (corresponding to the dilute limit); but in the  
136 alloys under consideration in this study, the Chromium content is usually  
137 large as will be discussed further below (section 4).

The substitution energy of each element was calculated as

$$E_{X,\gamma} = E(\text{Ni}_{31}\text{X}) - (31E(\text{Ni}) + E(\text{X})) \quad (1)$$

138 where  $E(\ )$  denotes the calculated energy of the structure or element.

## 139 2.4 Substitution in the $\delta$ -phase

140 Calculations for the pure  $\delta$ -phase ( $\text{Ni}_3\text{Nb}$ ) were done with a 32-atom super-  
141 cell configuration taken from the open quantum molecular database OQMD  
142 [16]. The structure was relaxed as explained in section 2.1. Spin-polarized  
143 calculations were performed to check that the calculated end-state was un-  
144 magnetic.

145 To calculate alloying effects for the alloying elements under consideration,  
146 one atom in the supercell was replaced. There are three distinct possibilities  
147 to substitute one atom in the  $\delta$ -phase, as calculated with SOD [18]: two for  
148 substituting Ni, one for Nb. These configurations are shown in Fig. 1. For  
149 each calculation, the lattice relaxation algorithm from section 2.1 was used.

150 All calculations were spin-polarized (starting from a ferro-magnetic cell)  
151 to check whether magnetic effects might play a role. For those elements  
152 where atoms in the final configuration possessed a non-negligible magnetic  
153 moment, non-polarized calculations were also performed to see the strength  
154 of the effect.

The solution energy for an element in the  $\delta$ -phase is calculated using the  
 $\delta$ -phase, the pure  $\gamma$ -phase and the pure element as a reference state. The  
energy depends on where the solution element is situated in the lattice. If the  
atom sits on a Nb position, dissolving it in the  $\delta$ -phase requires to transfer  
three Ni atoms from the  $\gamma$  to the  $\delta$ -phase because the Nb atom has the lowest  
energy in the  $\delta$ -phase and will thus not shift to another phase. To replace Ni,  
a single Ni atom is shifted from the  $\delta$  to the  $\gamma$ -phase. The solution energies  
are therefore calculated as

$$E_{X,\delta,\text{Nb}} = E(\text{Ni}_{24}\text{Nb}_7\text{X}) - (7E(\text{Ni}_3\text{Nb}) + 3E(\text{Ni}) + E(\text{X})) \quad (2)$$

$$E_{X,\delta,\text{Ni}} = E(\text{Ni}_{23}\text{Nb}_8\text{X}) + E(\text{Ni}) - (E(\text{Ni}_{24}\text{Nb}_8) + E(\text{X})) . \quad (3)$$

To see whether an element dissolves in the  $\gamma$ - or in the  $\delta$ -phase, the

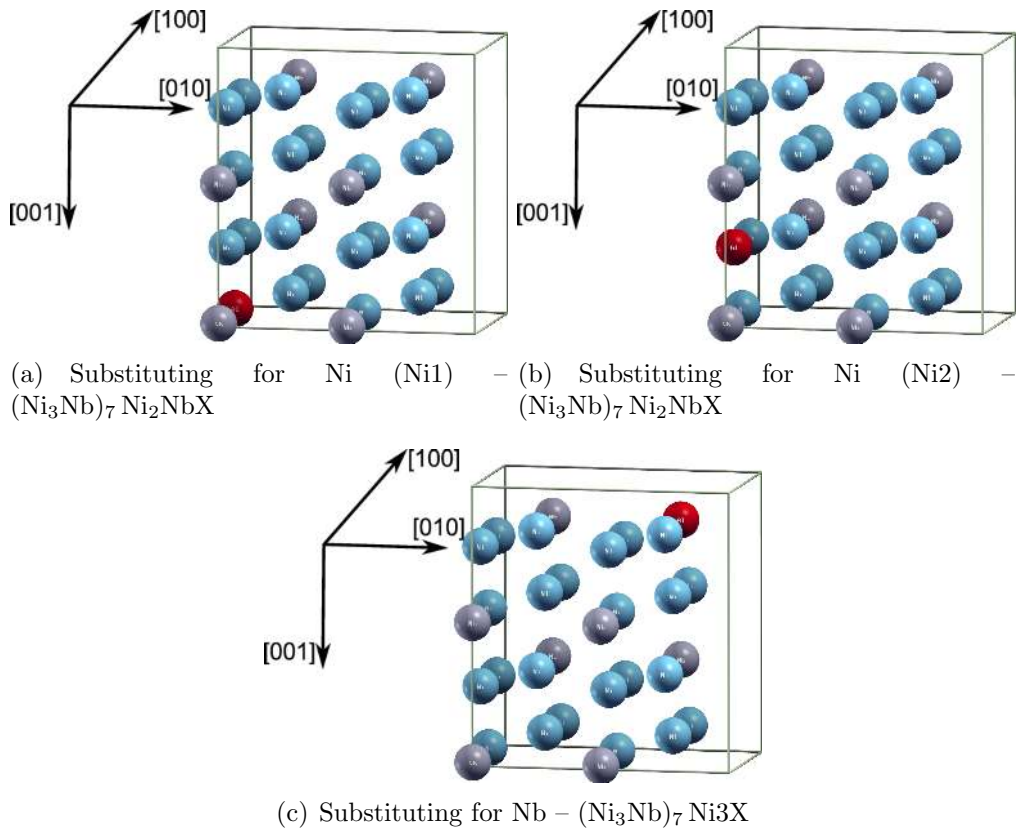


Figure 1: Substitution of one alloying atom for Ni or Nb in the  $\delta$  phase (Ni atoms in blue, Nb atoms in grey, alloying atom in red).



difference in the solution energies is calculated:

$$\begin{aligned} E_{X,\text{Diff}, \delta, \text{Nb}} &= E_{X,\delta, \text{Nb}} - E_{X,\gamma} \\ &= E(\text{Ni}_{24}\text{Nb}_7\text{X}) + 28E(\text{Ni}) - 7E(\text{Ni}_3\text{Nb}) - E(\text{Ni}_{31}\text{X}) \end{aligned} \quad (4)$$

$$\begin{aligned} E_{X,\text{Diff}, \delta, \text{Ni}} &= E_{X,\delta, \text{Ni}} - E_{X,\gamma} \\ &= E(\text{Ni}_{23}\text{Nb}_8\text{X}) + 32E(\text{Ni}) - E(\text{Ni}_{24}\text{Nb}_8) - E(\text{Ni}_{31}\text{X}). \end{aligned} \quad (5)$$

## 155 2.5 Substitution in the $\eta$ -phase

156 The strategy for the calculations of the  $\eta$ -phase was the same as for the  
 157  $\delta$ -phase. The initial configuration was again taken from the OQMD and  
 158 relaxed. Afterwards, substitutions of the alloying elements were calculated.  
 159 Fig. 2 shows the possible replacements in the 32-atom cell of the  $\eta$ -phase  
 160 (two each for the Ti and the Ni substitution).

161 The  $\eta$ -phase itself was found to be unmagnetic, but there are magnetic ef-  
 162 fects for several alloying elements. For these, non-spin-polarized calculations  
 163 were performed as well.

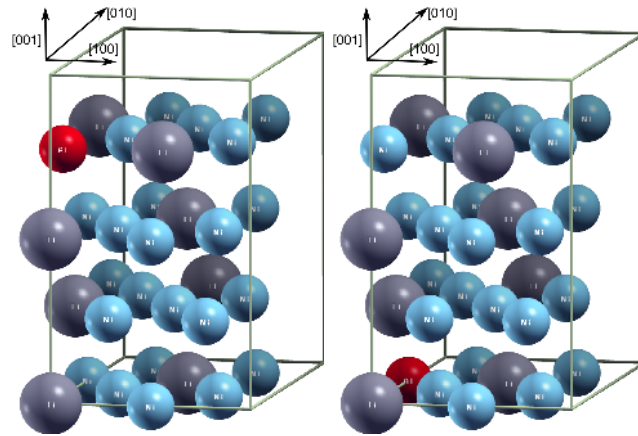
164 Solution energies were calculated in the same way as for the  $\delta$ -phase, see  
 165 eqs. (2)–(5), replacing Ti for Nb.

## 166 3 Results

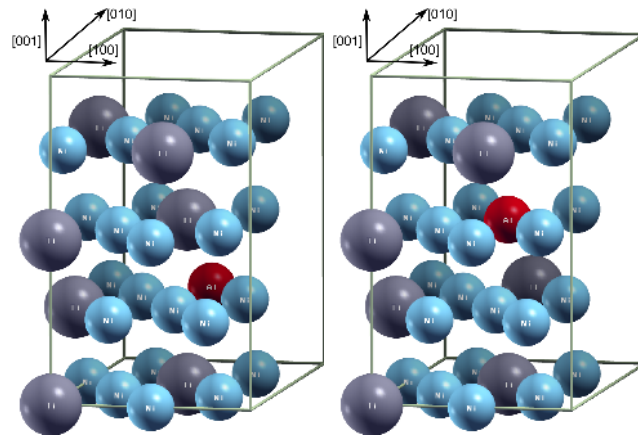
### 167 3.1 Pure elements

168 Table 1 shows the calculated energy per atom for each of the considered ele-  
 169 ments. For those elements were calculations with the same pseudopotential  
 170 were available in the OQMD [16], agreement between our calculations and the  
 171 OQMD results was usually within less than 3 meV. Exceptions were elements  
 172 for which our lattice relaxation method yields considerably different lattice  
 173 constants (Ag, Cd, Au, Hg). For these elements, deviations in the energies  
 174 of up to 17 meV occurred, and lattice parameters differed by 1% or more.  
 175 Since the OQMD results were obtained using a direct relaxation of the cell  
 176 size in a single calculation, this difference can be explained by the different  
 177 calculation method to obtain the relaxed ground state (see section 2.1).

178 For Pd, initializing with a ferromagnetic state results in an end state with  
 179 a small magnetic moment on each Pd atom. The energy of this structure is



(a) Substituting for Ni (Ni1) –  $(\text{Ni}_3\text{Ti})_3\text{Ni}_2\text{TiX}$       (b) Substituting for Ni (Ni2) –  $(\text{Ni}_3\text{Ti})_3\text{Ni}_2\text{TiX}$



(c) Substituting for Ti (Ti1) –  $(\text{Ni}_3\text{Ti})_3\text{Ni}_3\text{X}$       (d) Substituting for Ti (Ti2) –  $(\text{Ni}_3\text{Ti})_3\text{Ni}_3\text{X}$

Figure 2: Substitution of one alloying atom for Ni or Ti in the  $\eta$  phase (Ni atoms in blue, Ti atoms in grey, alloying atom in red).

Table 1: Calculated energy per atom of the pure alloying elements.

<b>Element</b>	<b>structure</b>	<b>Energy / eV/atom</b>
Al	fcc	-3.7461
Ti	hcp	-7.9461
V	bcc	-9.1193
Cr	bcc	-9.6462
Mn	cub	-9.1528
Fe	bcc	-8.4568
Co	hcp	-7.1084
	fcc	-7.0906
Ni	fcc	-5.7792
Cu	fcc	-4.0985
Zn	hcp	-1.2660
Zr	hcp	-8.5471
Nb	bcc	-10.2252
Mo	bcc	-10.8490
Tc	hcp	-10.3622
Ru	hcp	-10.3622
Rh	fcc	-7.3445
Pd	fcc	-5.3860
Ag	fcc	-2.8283
Cd	hcp	-0.8865
Hf	hcp	-9.9560
Ta	bcc	-11.8531
W	bcc	-12.9613
Re	hcp	-12.4461
Os	hcp	-11.2266
Ir	fcc	-8.8573
Pt	fcc	-6.0571
Au	fcc	-3.2723
Hg	rhl	-0.2956

180 1.7 meV lower than the energy of a Pd atom in a non-spin-polarized calculation.  
 181 In the calculations of the substitution energies, the lower energy value  
 182 was used. For Co, both an fcc and an hcp structure were calculated because  
 183 the energy of both phases is known to be very similar. In our calculation,  
 184 the energy of the hcp is slightly smaller than that of the fcc structure.

185 Note that the results of the pure element energies are relevant for the  
 186 substitution energies, but not for a comparison of these energies (the question  
 187 whether an element would transfer to  $\delta/\eta$  from  $\gamma$ ).

## 188 3.2 $\gamma$ -phase

189 The energy of a nickel atom of the pure  $\gamma$ -phase is reported in Table. 1; the  
 190 calculated lattice constant was 3.523 Å. Substituting one nickel atom by an  
 191 alloying element in the 32-atom supercell corresponds to a concentration of  
 192 3.125%. The calculated change in the lattice constant can be used to predict  
 193 the influence of the alloying elements on the lattice constant. In Fig. 3, the  
 194 change in the lattice constant is shown for all elements and compared with  
 195 data from [19] where data is available. With the exception of Os, the agree-  
 196 ment between the calculation and the experimental results is satisfactory.

197  
 198 The calculated substitution energies for all elements in the  $\gamma$ -phase are  
 199 shown in Fig. 4. Positive values in the diagram do not imply that the con-  
 200 sidered element cannot be used in alloying because many of the transition  
 201 element have a finite solubility in nickel at typical processing temperatures  
 202 of the order of 1000 °C.

## 203 3.3 $\delta$ -phase

To check whether the  $\delta$ -phase is stable, we calculate the energy of  $\text{Ni}_3 + \text{Nb}$   
 in three different states (dissolved in  $\gamma$ , as a  $\delta$  cell or as isolated nickel and  
 niobium phases):

$$\begin{aligned}
 E_{\text{solution}} &= E(\text{Ni}_{31}\text{Nb}) - 28E(\text{Ni}) &= -28.2496 \text{ eV} \\
 E_{\delta} &= \frac{1}{8}E(\text{Ni}_{24}\text{Nb}_8) &= -28.8134 \text{ eV} \\
 E_{\text{separated}} &= E(\text{Nb}) + 3E(\text{Ni}) &= -27.4329 \text{ eV} .
 \end{aligned}$$

204 Formation of the  $\delta$ -phase from the  $\gamma$ -phase is thus energetically favorable by  
 205 564 meV per Niobium atom. Note that other phases (like NiNb) were not

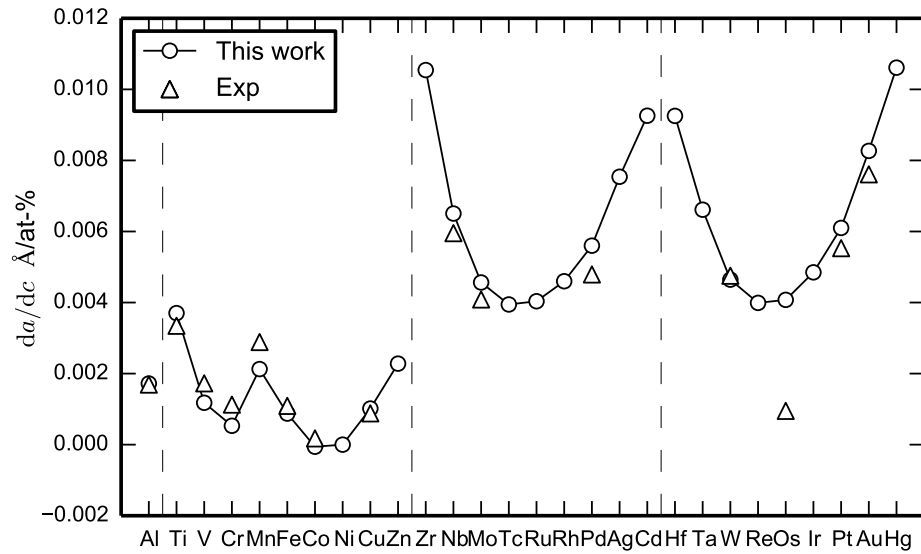


Figure 3: Predicted change in the lattice constant (in  $\text{\AA}$ ) per at.-% of an alloying element ( $da/dc$ ) compared to the experimental results reported in [19].

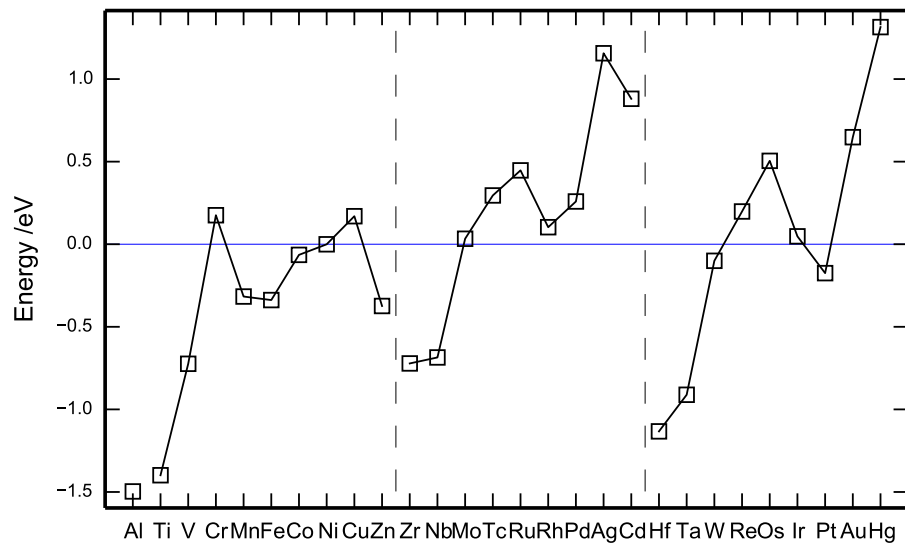


Figure 4: Substitution energies for the considered alloying elements in the  $\gamma$ -phase, calculated from eq. (1)

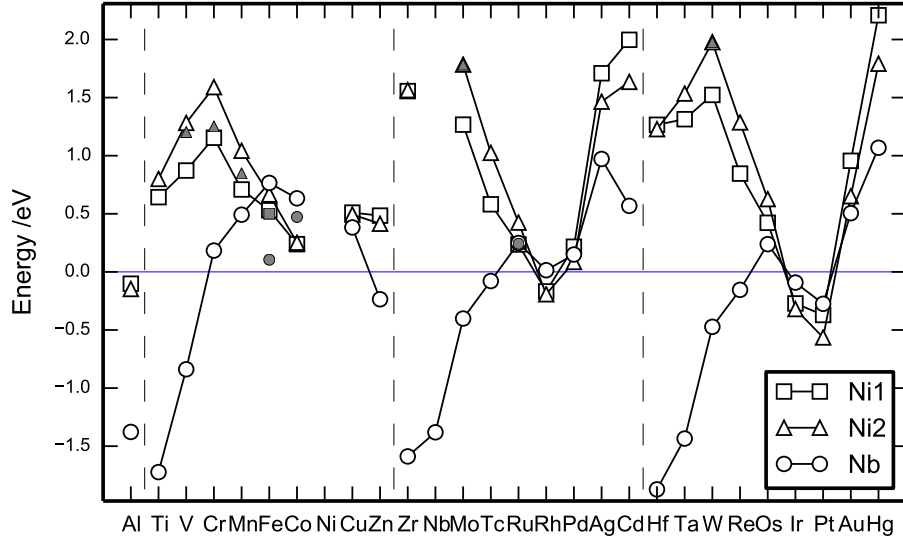


Figure 5: Substitution energies for an element in the  $\delta$ -phase, calculated from eqs. (2) and (3). Grey symbols denote lowest-energy states with a magnetic moment in the  $\delta$ -phase. For Nb, the energy difference between the  $\delta$ -phase and the separate pure Ni and Nb phases has been plotted.

206 considered here because they do not occur in the alloys under consideration,  
 207 so the stability is only shown with respect to pure Nb and solution in the  
 208  $\gamma$ -phase. As expected, the  $\delta$ -phase was unmagnetic.

209 The calculated lattice constants of the  $\delta$ -phase were 5.123 Å, 4.258 Å,  
 210 and 4.562 Å. These values agree to within 1% with measured values from the  
 211 literature [20] and with other DFT calculations [21].

212 Fig. 5 shows the substitution energies of the considered elements (using  
 213 the pure  $\delta$ -phase, pure nickel and the pure element as a reference state),  
 214 calculated from eqs. (2) and (3). For some elements a non-zero magnetic  
 215 moment was found as lowest energy state in the 32-atom  $\delta$ -supercell. For  
 216 these elements, an additional non-spin-polarized calculation (including lattice  
 217 relaxation) was performed. The energy of the magnetic state is shown in the  
 218 Figure (grey symbols). The substitution of a nickel atom in the  $\delta$ -phase  
 219 becomes energetically more favourable with increasing number of  $d$ -electrons  
 220 as should be expected. The energy rises again if the number of  $d$ -electrons

Table 2: Predicted substitution behaviour in the  $\delta$ -phase of different elements from [22] compared to the DFT calculations from figure 6. For iron, the calculated lowest energy state depends on whether a ferromagnetic (replace Nb) or a non-ferromagnetic state (replace Ni) in the  $\delta$ -phase is considered.

	Al	Ti	V	Cr	Mn	Fe	Co	Cu			
[22]	Nb	Nb	Nb	Nb	Nb	Ni/Nb	Ni	Nb			
This work	Nb	Nb	Nb	Nb	Nb	Ni/Nb	Ni	Nb			
	Zr	Mo	Pd	Hf	Ta	W	Re	Os	Ir	Pt	Au
[22]	Nb	Nb	Ni	Nb	Nb	Nb	Ni	Ni	Ni	Ni	Ni
This work	Nb	Nb	Ni	Nb	Nb	Nb	Nb	Nb	Ni	Ni	Nb

221 is larger than that of nickel. Substituting Nb is favorable for elements with  
 222 a low number of  $d$ -electrons.

223 In [22], a thermodynamic model was used to determine the solution be-  
 224 haviour of several elements in different  $\text{Ni}_3\text{M}$  phases. The model was used  
 225 to predict whether solution elements are situated on Ni or Nb sites in the  
 226  $\delta$ -phase. Table 2 shows a comparison between the predictions of [22] and  
 227 the current work for the site preference of the elements. For most of the ele-  
 228 ments, predictions do agree, but there is a discrepancy for Re, Os, and Au.  
 229 For Os and Au, the calculated energy differences are small, but the difference  
 230 is large for Re.

231 Fig. 6 shows the energy of transferring an alloying element from the  $\gamma$   
 232 to the  $\delta$ -phase in a Ni or Nb position. (Data points in this figure can be  
 233 obtained as difference between the results from Fig. 4 and Fig. 5.) Overall,  
 234 substituting nickel in the  $\delta$ -phase is not favoured for any of the elements in  
 235 the Ti-period. In the higher periods, substituting nickel is favourable for  
 236 Ru, Rh, Pd, Os, Ir, and Pt. From Fig. 5, it might seem that some of these  
 237 elements (Ru, Pd, and Os) would not dissolve in the  $\gamma$  or the  $\delta$ -phase, but at  
 238 finite temperatures, these elements have a finite solubility in the  $\gamma$  matrix.  
 239 During formation of the  $\delta$ -phase, these elements may then be expected to  
 240 dissolve in the more favourable phase.

241 On the other hand, elements with a low number of  $d$ -electrons, especially  
 242 those in higher periods, can replace a niobium atom. (Note that the energy  
 243 gain of the  $\delta$ -phase formation has been entered into the figure in the Nb  
 244 position.) It has to be noted, however, that these elements may form other  
 245 phases like  $\text{Ni}_3\text{Ti}$ .



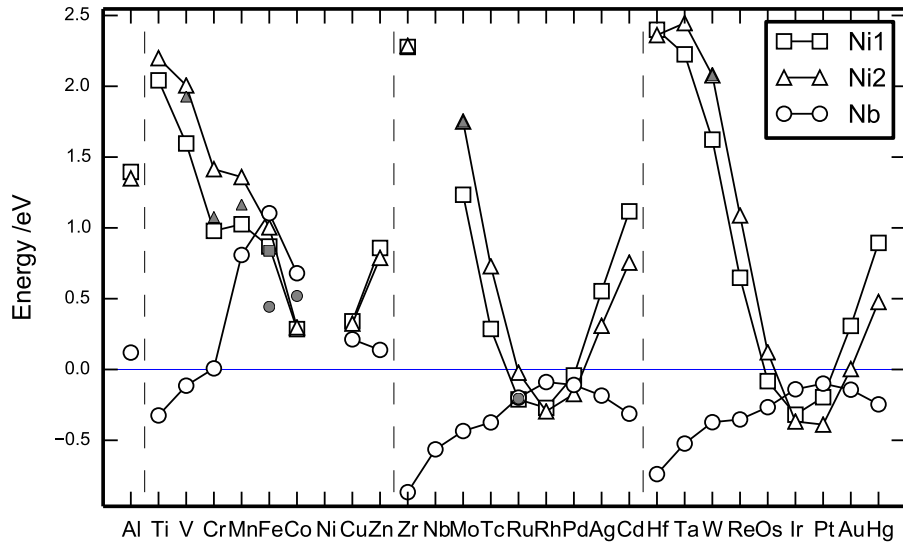


Figure 6: Energy difference between an alloying element in the  $\delta$  and in the  $\gamma$ -phase, calculated from eqs. (4) and (5). For Nb, the energy difference between the  $\delta$ -phase and a dissolved Nb in the  $\gamma$ -phase is shown. Grey symbols denote lowest-energy states with a magnetic moment in the  $\delta$ -phase.

246 For most of those elements where a non-zero magnetic moment was found  
 247 as lowest energy state in the 32-atom  $\delta$ -supercell, the substitution energy for  
 248 a transfer from  $\gamma$  to  $\delta$  remains positive so that this effect will not affect  
 249 the solution behaviour. The only exception is Ru where the magnetic state  
 250 lowers the energy by only 6.6 meV.

### 251 3.4 $\eta$ -phase

We calculated the stability of the  $\eta$ -phase in the same way as for the  $\delta$ -phase;  
 again disregarding other phases like NiTi:

$$\begin{aligned}
 E_{\text{solution}} &= E(\text{Ni}_{31}\text{Ti}) - 28E(\text{Ni}) &&= -26.6836 \text{ eV} \\
 E_{\delta} &= \frac{1}{8}E(\text{Ni}_{24}\text{Ti}_8) &&= -27.2239 \text{ eV} \\
 E_{\text{separated}} &= E(\text{Ti}) + 3E(\text{Ni}) &&= -25.2850 \text{ eV}.
 \end{aligned}$$

252 Formation of the  $\eta$ -phase from the  $\gamma$ -phase is thus energetically favorable by  
 253 540 meV per titanium atom.

254 The calculated lattice constants for the conventional 32-atom unit cell  
 255 were  $a = 5.116 \text{ \AA}$  in the basal plane and  $c = 8.346 \text{ \AA}$ , close to the values of  
 256  $5.115 \text{ \AA}$  and  $8.302 \text{ \AA}$  given in [23].

257 Fig. 7 shows the substitution energies of the considered elements (using  
 258 the pure  $\delta$ -phase, pure nickel and the pure element as a reference state),  
 259 calculated in the same way as for the  $\delta$ -phase. A ferromagnetic state was  
 260 found as ground state for several elements (marked by grey symbols in Fig. 7).  
 261 The effect is especially strong for Cr, Mn, Fe, and Co in a Ti position of the  
 262  $\eta$ -phase, where the energy is lowered considerably.

263 Fig. 8 shows the energy of transferring an alloying element from the  $\gamma$  to  
 264 the  $\eta$ -phase in a Ni or Ti position. The overall shape of the curves is similar  
 265 to those for the  $\delta$ -phase. Substituting a nickel atom in the  $\eta$ -phase is most  
 266 favourable for atoms with a similar number of  $d$ -electrons, but only Ru, Rh,  
 267 Pd, Ir, and Pt can be expected to actually stabilize the  $\eta$ -phase in this way.  
 268 Substituting Ti is favourable for Al, Zn, Zr, Nb, Cd, Hf, Ta and Hg. A slight  
 269 stabilization effect might be expected for V, Mo, Ag, and W, but the energies  
 270 are small compared to typical thermal energies at the forging temperature.

271 Ferromagnetic effects in the  $\eta$ -phase are especially strong for Cr, Mn, Fe,  
 272 and Co in a Ti position of the  $\eta$ -phase. For Cr and Mn, the energy to trans-  
 273 fer an atom to the  $\eta$ -phase energy becomes slightly negative (of the order

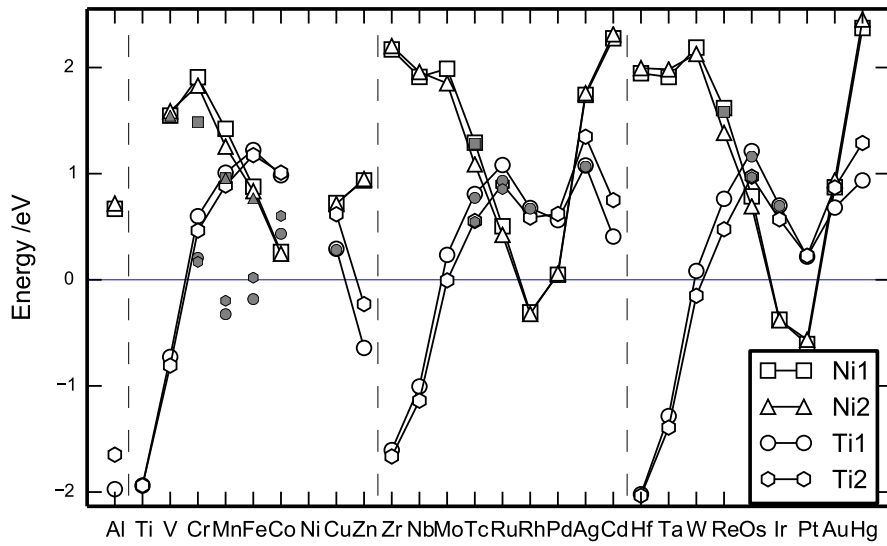


Figure 7: Substitution energies for an element in the  $\eta$ -phase, calculated from eqs. (2) and (3). Grey symbols denote lowest-energy states with a magnetic moment in the  $\eta$ -phase. For Ti, the energy difference between the  $\eta$ -phase and the separate pure Ni and Ti phases has been plotted.

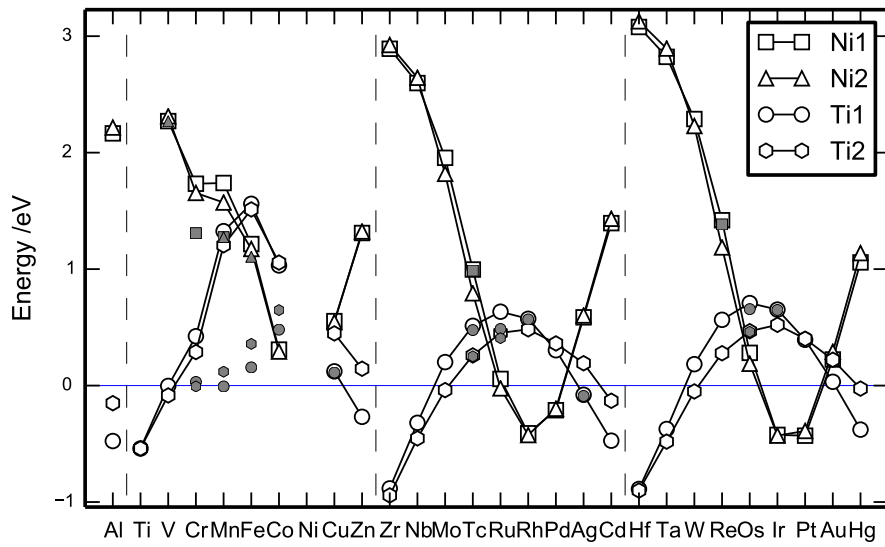


Figure 8: Energy difference between an alloying element in the  $\eta$  and in the  $\gamma$ -phase, calculated from eqs. (4) and (5); replacing Ti for Nb. For Ti, the energy difference between the  $\eta$ -phase and a dissolved Ti in the  $\gamma$ -phase is shown. Grey symbols denote lowest-energy states with a magnetic moment in the  $\eta$ -phase.

274 of 7 meV). These magnetic effects might become even stronger if the con-  
275 centration of these alloying elements is increased further and these elements  
276 then might actually stabilize the  $\eta$ -phase. A similar effect may also occur for  
277 Fe and Co in higher concentrations in the  $\eta$ -phase. For the other elements  
278 where a magnetic state was found, the effect is small and probably does not  
279 affect the energies significantly.

## 280 4 Discussion

281 As explained in the introduction, the  $\delta$  and  $\eta$ -phase are important in design-  
282 ing wrought alloys. For some alloys (like alloy 718), stabilizing the  $\delta$ -phase  
283 at higher temperatures without simultaneously promoting the  $\eta$ -phase is an  
284 important goal, whereas other alloys like alloy 706 exploit the  $\eta$ -phase. It is  
285 therefore important to understand which elements may be used to selectively  
286 stabilize one of these phases.

287 Fig. 9 shows a plot of the calculated energies from Fig. 6 and 8. The two  
288 shaded regions show which elements can be used to stabilize one phase more  
289 strongly than the other, with elements close to the boundary between the  
290 regions stabilizing both phases.

291 Elements that strongly favor the  $\delta$ -phase are Mo, Tc, Re, Os, and W.  
292 The elements V, Ta, Ru, Ag, and Au also stabilize the  $\delta$ -phase more strongly  
293 than the  $\eta$ -phase, but the effect is of the order of the thermal energy at  
294 forging temperature ( $k_B T \approx 100$  meV). The  $\eta$ -phase is strongly stabilized  
295 by Al and Zn. For Cd, Rh, and Hg, the energy in the  $\eta$ -phase is close to  
296 that in the  $\delta$ -phase so that both phases may be stabilized. This is also  
297 true for Zr and Hf which have a strong tendency to replace Nb and Ti,  
298 respectively. (At sufficiently high concentrations,  $\text{Ni}_3\text{Zr}$  or  $\text{Ni}_3\text{Hf}$  may form  
299 instead.) Note that among these elements, Hg, Cd, Ag, Au are known to  
300 strongly deteriorate mechanical properties of the alloys and are thus not  
301 suitable as alloying elements.

302 Although the  $\delta$  and  $\eta$ -phase are non-magnetic, alloying elements may  
303 change the magnetic state of these phases. This effect is largest for Cr, Mn,  
304 Fe, and Co. For the  $\delta$ -phase, these elements have large energies in the  $\delta$ -  
305 phase and do not dissolve in this phase according to our calculations, but for  
306 the  $\eta$ -phase, magnetic effects may actually allow these elements to dissolve.  
307 It can also be expected that increasing the concentration of these elements  
308 will increase this effect further.

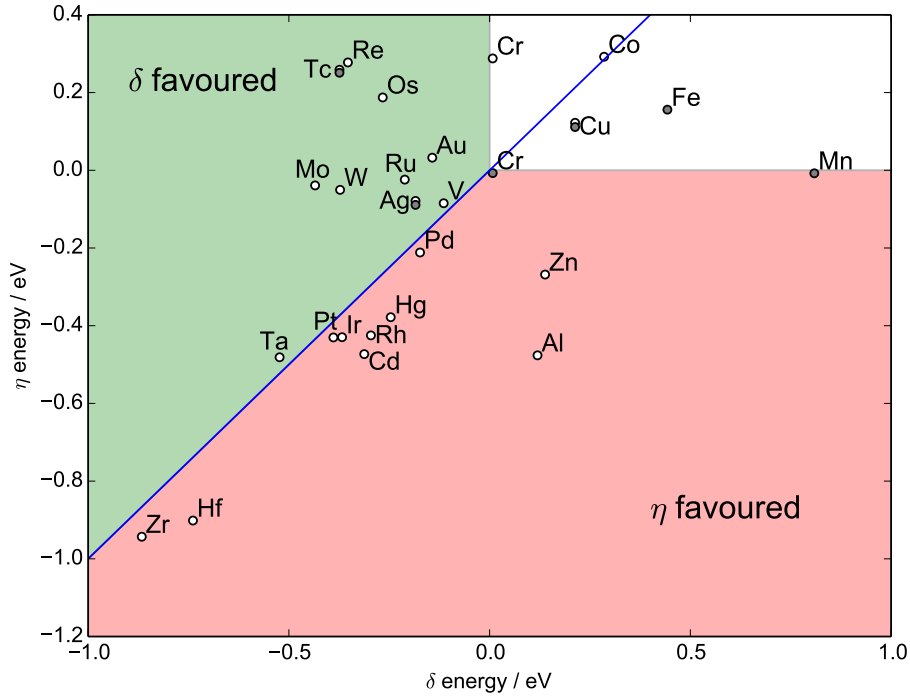


Figure 9: Effect of alloying elements on the stability of the  $\delta$ -phase and  $\eta$ -phase. The plot shows the energy change in adding an element to both phases. Elements in the upper left region tend to stabilize the  $\delta$ -phase more strongly than the  $\eta$ -phase; those in the lower right region stabilize the  $\eta$ -phase more strongly. Datapoints in grey are for configurations with magnetic moment in the  $\delta$  or  $\eta$ -phase; datapoints for the non-magnetic state of Fe and Mn in the  $\eta$ -phase are not shown because they are outside of the scale (larger than 1 eV).

309 In the calculations presented here, a  $\text{Ni}_{31}\text{X}$ -supercell was used to represent  
310 the  $\gamma$ -phase. In realistic nickelbase superalloys, the  $\gamma$ -phase contains a large  
311 number of alloying elements. One of these elements is chromium which has  
312 the effect of making the alloy non-ferromagnetic. A full study of a 32-atom  
313 supercell with the appropriate amount of Cr-atoms (typical Cr contents are  
314 about 18%) would require the computation of a large number of different  
315 configurations and is beyond the scope of this paper. To estimate the size  
316 of the effect, we performed some preliminary calculations using a smaller  
317  $\text{Ni}_{14}\text{Cr}_2$  cell. We chose the lowest-energy state we found for this cell as  
318 a reference and then substituted one Ni atom by the alloying element in  
319 different positions. The solution energies of most elements tend to decrease  
320 on the order of about 200 meV, so that dissolving elements in the chromium-  
321 containing matrix becomes more favourable. Thus it may be expected that  
322 the phase-strengthening effect of some elements may be weakened by this  
323 effect. A more detailed study of this effect will be done in the future.

324 In conclusion, our results give theoretical insights into the stabilizing  
325 effects of relevant alloying elements on the  $\delta$  and  $\eta$ -phase. All calculations  
326 were performed at 0 K. Additional studies are thus necessary to see how finite-  
327 temperature effects affect our results. In addition, EDX-measurements of the  
328  $\delta$  and  $\eta$ -phase will be performed to compare these results to experiments.

## 329 Acknowledgements

330 The DFT simulations were performed with resources provided by the North-  
331 German Supercomputing Alliance (HLRN).

## 332 References

- 333 [1] WD Kennedy and RL Cao. New development in wrought in 718-type.  
334 *Acta Metall*, 18(1):39–46, 2005.
- 335 [2] Xi Shan Xie, Jian Xin Dong, and Mai Cang Zhang. Research and de-  
336 velopment of Inconel 718 type superalloy. In *Materials science forum*,  
337 volume 539, pages 262–269. Trans Tech Publ, 2007.

- 338 [3] Robert E Schafrik, Douglas D Ward, and Jon R Groh. Application  
339 of alloy 718 in GE aircraft engines: past, present and next five years.  
340 *Superalloys*, 718:625–706, 2001.
- 341 [4] Peter W Schilke, JJ Pepe, and Robin C Schwant. Alloy 706 metallurgy  
342 and turbine wheel application. *Superalloys*, 718(625,706):1, 1994.
- 343 [5] RL Kennedy. ALLVAC® 718PLUS™, superalloy for the next forty  
344 years. *Superalloys*, 718:625–706, 2005.
- 345 [6] T Fedorova, J Rösler, B Gehrman, and J Klöwer. Invention of a New  
346 718-Type Ni-Co Superalloy Family for High Temperature Applications  
347 at 750 C. In *8th International Symposium on Superalloy 718 and Deriva-*  
348 *tives*, pages 587–599. Wiley Online Library, 2014.
- 349 [7] Xiaoxia Wu and Chongyu Wang. Density functional theory study of the  
350 thermodynamic and elastic properties of Ni-based superalloys. *Journal*  
351 *of Physics: Condensed Matter*, 27(29):295401, 2015.
- 352 [8] G Kresse and J Hafner. Ab initio molecular-dynamics simulation of the  
353 liquid-metal–amorphous-semiconductor transition in germanium. *Phys-*  
354 *ical Review B*, 49(20):14251, 1994.
- 355 [9] Georg Kresse and Jürgen Furthmüller. Efficient iterative schemes for  
356 ab initio total-energy calculations using a plane-wave basis set. *Physical*  
357 *Review B*, 54(16):11169, 1996.
- 358 [10] Georg Kresse and Jürgen Furthmüller. Efficiency of ab-initio total en-  
359 ergy calculations for metals and semiconductors using a plane-wave basis  
360 set. *Computational Materials Science*, 6(1):15–50, 1996.
- 361 [11] Peter E Blöchl. Projector augmented-wave method. *Physical Review B*,  
362 50(24):17953, 1994.
- 363 [12] Georg Kresse and D Joubert. From ultrasoft pseudopotentials to the  
364 projector augmented-wave method. *Physical Review B*, 59(3):1758, 1999.
- 365 [13] John P Perdew, Kieron Burke, and Matthias Ernzerhof. Generalized gra-  
366 dient approximation made simple. *Physical review letters*, 77(18):3865,  
367 1996.



- 368 [14] G Kresse and O Lebacqz. Vasp manual, 2013.
- 369 [15] Francis Birch. Finite elastic strain of cubic crystals. *Physical Review*,  
370 71(11):809, 1947.
- 371 [16] James E Saal, Scott Kirklin, Muratahan Aykol, Bryce Meredig, and  
372 Christopher Wolverton. Materials design and discovery with high-  
373 throughput density functional theory: the open quantum materials  
374 database (OQMD). *Jom*, 65(11):1501–1509, 2013.
- 375 [17] Stefano Curtarolo, Wahyu Setyawan, Shidong Wang, Junkai Xue,  
376 Kesong Yang, Richard H Taylor, Lance J Nelson, Gus LW Hart, Stefano  
377 Sanvito, Marco Buongiorno-Nardelli, et al. AFLOWLIB. ORG: A dis-  
378 tributed materials properties repository from high-throughput ab initio  
379 calculations. *Computational Materials Science*, 58:227–235, 2012.
- 380 [18] R Grau-Crespo, S Hamad, CRA Catlow, and NH De Leeuw. Symmetry-  
381 adapted configurational modelling of fractional site occupancy in solids.  
382 *Journal of Physics: Condensed Matter*, 19(25):256201, 2007.
- 383 [19] AK Jena and MC Chaturvedi. The role of alloying elements in the design  
384 of nickel-base superalloys. *Journal of Materials Science*, 19(10):3121–  
385 3139, 1984.
- 386 [20] C Slama and M Abdellaoui. Structural characterization of the aged  
387 Inconel 718. *Journal of alloys and compounds*, 306(1):277–284, 2000.
- 388 [21] Zahra Tarzimoghadam, Michael Rohwerder, Sergiy Vasil Merzlikin, Asif  
389 Bashir, L Yedra, S Eswara, Dirk Ponge, and Dierk Raabe. Multi-scale  
390 and spatially resolved hydrogen mapping in a Ni–Nb model alloy reveals  
391 the role of the  $\delta$  phase in hydrogen embrittlement of alloy 718. *Acta*  
392 *Materialia*, 109:69–81, 2016.
- 393 [22] H Sugimura, Y Kaneno, and T Takasugi. Alloying Behavior of  
394 Ni3M-Type Compounds with D0a Structure. *Materials transactions*,  
395 52(4):663–671, 2011.
- 396 [23] Yoon-Uk Heo, Masaki Takeguchi, Kazuo Furuya, and Hu-Chul Lee.  
397 Transformation of DO 24  $\eta$ -Ni<sub>3</sub>Ti phase to face-centered cubic austenite  
398 during isothermal aging of an Fe–Ni–Ti alloy. *Acta Materialia*,  
399 57(4):1176–1187, 2009.